Tectonophysics 475 (2009) 554–562

Contents lists available at ScienceDirect

Tectonophysics

journal homepage: www.elsevier.com/locate/tecto

Quantification of fabrics in clay gouge from the Carboneras fault, Spain and implications for fault behavior

John G. Solum *, Ben A. van der Pluijm

University of Michigan, Department of Geological Sciences, 1100 N University Avenue, Ann Arbor, Michigan 48109-1003, United States

ARTICLE INFO

Article history:
Received 11 December 2008
Received in revised form 24 June 2009
Accepted 6 July 2009
Available online 15 July 2009

Keywords:
Fault mechanics
Permeability
Clay authigenesis
Fault strength

ABSTRACT

Clays in fault rocks have the potential to control fault behavior. The formation of frictionally-weak clays in fault rocks can lead to fault zone weakening, and the development of fabrics through authigenesis and mechanical rotation in clay-rich fault rocks can influence fault-zone permeability structures. The left lateral Carboneras Fault of southwestern Spain is a ca. 1 km wide fault zone with anastomosing layers of clay-rich gouge up to ~50 m thick. The gouge, derived largely from mica schist, is composed of neoformed illite and chlorite. Anisotropy of magnetic susceptibility (201 measurements) and X-ray pole figures (144 measurements) show comparable oblate clay fabrics, with the axis of maximum anisotropy sub-parallel to strike. This dimensional fabric contrasts with previously published maximum permeability results that are sub-vertical. This observation, coupled with the generally poor clay fabric measured in the samples indicates that the orientation of clays is not likely to be the primary control of the permeability anisotropy of clay-rich fault gouge, becoming important only when gouge zones are 10s of meters thick, which is very unusual. Even in a fault zone like that of the Carboneras fault, with thick, very clay-rich gouge zones with a visible foliations and slip surfaces, the degree of clay preferred orientation is low above the millimeter scale, showing that any strong clay fabric associated with the foliation are extremely localized phenomena. This suggests that processes operating below the millimeter scale may significantly influence fault behavior, a result compatible with earlier characterizations of faults in a variety of geologic settings, highlighting the importance of understanding how the formation and fabric of fault-related authigenic clays influence fault behavior.

1. Introduction

1.1. Geologic setting

The Carboneras Fault zone in Almeria Province in southern Spain (Fig. 1) is a crustal-scale strike slip fault that is part of the plate boundary between Iberia and Africa (Faulkner et al., 2003). It has accommodated ~40 km of sinistral offset, and has been exhumed from a depth of at least 1.5 km in an arid climate, which served to limit alteration/weathering of the fault zone (Faulkner et al., 2003). The Carboneras Fault juxtaposes Alpine crystalline protolith (mica schist, phyllite and quartzite derived from Permo-Triassic sediments) against Tertiary clastic and carbonate sedimentary and volcanic rocks. The fault zone is ~1 km wide and is characterized by anatomizing gouge zones that are up to ~50 m wide. The fault has been compared to the creeping segment of the San Andreas Fault (Faulkner et al., 2003), similar to the location of the SAFOD project (Hickman et al., 2005; Solum et al., 2005) and its excellent exposure and preservation provides an opportunity to study processes of clay fabric development in major fault systems that otherwise remain inaccessible at depth.

1.2. Background

The Carboneras Fault was selected for study as its permeability structure has been thoroughly investigated (Faulkner and Rutter, 1998, 2001). The illite/chlorite/quartz gouge has a maximum permeability of ~10^{-18} m^2 in the fault plane in a vertical direction, and a minimum permeability of ~10^{-21} m^2 perpendicular to the fault zone, measured using argon as a pore fluid at a confining pressure of 40 MPa (Faulkner and Rutter, 2001). Given these values of vertical and lateral permeability and the ~1 km width of the fault zone, vertical fluid flux would exceed lateral fluid flux, thereby allowing elevated fluid pressure (approaching lithostatic) to be maintained and weakening the fault (Faulkner and Rutter, 2001). Toward our fabric study of these rocks we developed a technique for creating thick sections from very clay-rich rocks and quantitatively evaluating fabrics using X-ray and rock magnetic techniques.

Clay fabrics in fault rocks can be difficult to characterize because of challenges with sample collection and preparation, and especially the

* Corresponding author. Present address: Shell International Exploration and Production, Inc., 3737 Bellaire Blvd., Houston, TX 77025, United States.
E-mail address: j.solum@shell.com (J.G. Solum).

0040-1951/$ – see front matter © 2009 Elsevier B.V. All rights reserved.
doi:10.1016/j.tecto.2009.07.006

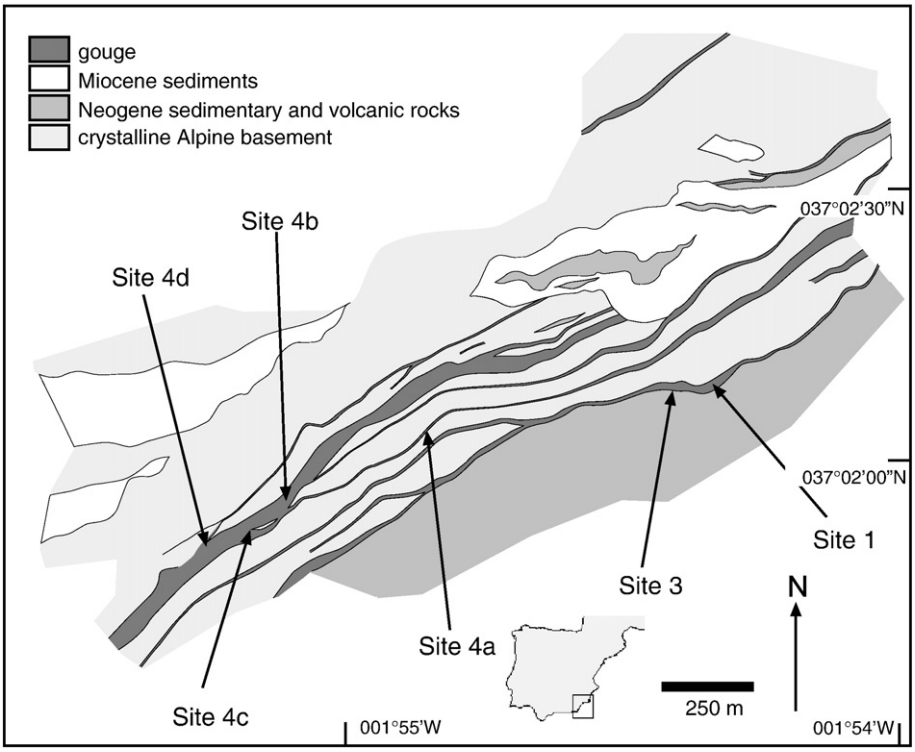

Fig. 1. Geologic map of the Carboneras fault, Spain. Inset map shows the location of the study site in southeastern Spain. Sample locations are shown by arrows. Simplified from Faulkner et al. (2003).

very fine grain size of clays, which can only be directly imaged using transmission electron microscopy (e.g., Yan et al., 2001; Solum et al., 2003). Despite these difficulties, it is vitally important to constrain the nature and the occurrence of clays in fault zones, as they can influence both the mechanical and hydrologic properties of fault zones. For example, characterizations of samples from the active San Andreas Fault suggest that thin layers of neoformed clays (specifically illite and mixed-layer illite–smectite) are common in that fault zone at depths of less than several kilometers (Schleicher et al., 2006; Solum et al., 2006;) and play a significant role in controlling the frictional properties of that fault at those depths (Tembe et al., 2006; Morrow et al., 2007), and possibly other fault zones (Saffer and Marone, 2003; Lockner et al., 2006). The Carboneras Fault has been compared to the creeping section of the San Andreas Fault (Faulkner et al., 2003) that was described in the studies given above.

The permeability structure of fault zones has been an area of active research, as elevated fluid pressure in fault zones was proposed as an explanation of mechanically weak fault behavior (Sibson, 1990; Blanpied et al., 1992; Rice, 1992; Byerlee, 1993), particularly for large faults at plate boundaries such as the San Andreas Fault system (Lachenbruch and Sass, 1980; Mount and Suppe, 1987; Zoback 2000), but also for large faults in general (Hubbert and Rubey, 1959; Sibson, 1990; Solum et al., 2005). Studies of natural (e.g., Evans et al., 1997; Morrow et al., 1984) and synthetic gouges (e.g., Zhang et al., 1999; Zhang and Cox, 2000) have been conducted, but quantitative characterizations of clay fabrics in natural and synthetic fault rocks that supported these inferences are rare (Solum et al., 2003; Hayman et al., 2003; Solum et al., 2005). Given the very common appearance of clays in fault rocks it is critical to 1) quantify the composition and fabric of fault-related clays and 2) determine the ways in which those clays influence fault behavior. The anisotropy of magnetic susceptibility provides information on fabrics at the cm scale while X-ray texture goniometry provides information on fabrics at the mm scale. Quantifying clay fabrics, and the scales over which they exist, is the focus of this study that quantitatively addresses the first question and inferentially addresses the second.

2. Methods

2.1. Sample collection and basic laboratory preparation

Oriented hand samples were collected from six locations along the fault zone (Fig. 1). Because of their fragility, samples were tightly wrapped in multiple layers of newspaper and tape, and stored in plastic bags with moist paper towels to prevent dehydration. Attempts were made to collect small cores using ~15 cm long sections of PVC pipe similar to the method used by Vrolijk and van der Pluijm (1999) along the Lewis Thrust in Alberta, Canada. Except where the gouge was fully water saturated, which was the case at only one location, the action of pounding the pipe into the outcrop destroyed the friable samples. Faulkner and Rutter (2001) successfully collected cores using thin walled metal pipe, but we did not employ this technique due to the difficulty in extracting the sample from the pipe in the laboratory. Three oriented hand samples of phyllosilicate bearing protolith (phyllite and schist) were collected for comparison with gouge samples.

In the laboratory all but the innermost layer of newspaper was removed, and this innermost layer was perforated. The sample was then wrapped in damp paper towels and placed atop a large sponge in a sealed plastic bag. Samples were allowed to hydrate for ~1 week before being prepared for X-ray diffraction (XRD), X-ray texture goniometry (XTG), and anisotropy of magnetic susceptibility (AMS), as described below.

2.2. Magnetic susceptibility

Two hundred and one samples (191 from gouge, 10 from protolith) were cut from 14 hand specimens. Hydrated gouge samples were cut using a utility knife to fit into 2 cm hollow plastic cubes, resulting in a sample volume of ~8 cm^3. Oriented hand samples of protolith were cored using a 2.5 cm diameter diamond drill bit in the laboratory and trimmed to a length of ~2.4 cm. Both anisotropy of magnetic

susceptibility (AMS) and temperature-dependent susceptibility were measured. AMS was measured for 201 samples in a Kappabridge KLY-2 magnetic susceptibility meter, using the measuring procedure by Jelinek (1976), which involves measuring susceptibility in 15 different positions. We used the statistical analysis of Tauxe (1998) to calculate AMS fabrics and describe the anisotropy using the parameters of Jelinek (1981). The magnetic parameters used include the magnetic lineation L (τ_1/τ_2), magnetic foliation F (τ_2/τ_3), corrected anisotropy degree P' ($\exp\sqrt{2[(\eta_1-\eta)^2+(\eta_2-\eta)^2+(\eta_3-\eta)^2]}$) and shape factor T ($(2\eta_2-\eta_1-\eta_3)/(\eta_1-\eta_3)$) where τ_1,τ_2, and τ_3 are the maximum, intermediate and minimum susceptibilities, η_1,η_2, and η_3 are the natural logarithms of the susceptibilities, and η is the mean of η_1,η_2, and η_3.

In order to determine the role of paramagnetic phases (clays), diamagnetic phases (quartz), or ferrimagnetic phases (hematite), the susceptibility of 13 representative samples was measured from −196 °C (the temperature of liquid nitrogen) to ~20 °C (room temperature) in a Bartington MS2W magnetic susceptibility meter with continuous water circulation around the coil to ensure constant coil temperature (Richter and van derPluijm, 1994; Pares and van der Pluijm, 2002). Prior to placement in the susceptibility meter, samples were placed in a freezer overnight to solidify the water in the sample, thereby minimizing damage to the sample that would occur if liquid water in the samples flash froze upon sample immersion in liquid nitrogen. In order to measure temperature-dependent magnetic susceptibility frozen samples were placed in a dewar containing liquid nitrogen and allowed to equilibrate for 1 h. The samples were then placed in the susceptibility meter, and measured at ~3.5 s intervals until they reached room temperature (~30 min).

2.3. X-ray texture goniometry

XTG samples were cut from hand samples of the same gouge that was sampled for AMS. Once cut, the samples were placed in a bath of sodium silicate solution (Fisher Brand Sodium Silicate Solution SS338-4) mixed ~1:1 with water and allowed to rest for ~1 week, after which the samples were removed and allowed to air dry for 5–7 days. Although immersion in the sodium silicate solution helps to consolidate clay-rich samples it does not fill fractures or large voids. Consequently, samples were set in a low viscosity epoxy resin with a pot life of ~30 min (Struers EPOFIX) under mild vacuum following sodium silicate treatment. The combination of these two techniques was found to produce samples that can be thinly sliced and polished without disaggregating.

Resin-impregnated samples were cut on an oil-cooled, low-speed diamond wafering saw. Two cuts perpendicular to the expected fabric (i.e., foliation) were made for each sample; one perpendicular to the fault surface and parallel to strike, and the other perpendicular to the fault surface and parallel to dip direction. Cut surfaces were polished using 600 grit to remove saw marks and ensure a flat surface, and were then mounted on standard petrographic glass slides using sticky wax (Kerr Manufacturing Company, part # 00625), an adhesive with a low melting temperature commonly used to prepare samples for transmission electron microscopy. Following mounting of the sample on the slide, 400–700 μm-thick sections were cut. These sections were then lightly polished using 600 grit to remove any saw marks and removed from the glass slide and placed into custom made aluminum holders for XTG analysis.

Samples were measured in a modified Enraf-Nonius CAD4 single crystal X-ray diffractometer with a molybdenum source and a beam diameter of 1 mm (van der Pluijm et al., 1994). The phases in the analyzed area (chlorite, illite and quartz) were identified through the collection of a standard 2θ diffractogram. Once a relevant phyllosilicate phase was identified the detector was moved to the position that corresponds with the *d*-value of that phase [1.4 nm for chlorite (001), 1.0 nm for illite (001) and 0.7 nm for chlorite (002)]. The sample was then rotated through 1296 positions, with a count time at each position of 2 s. When the analysis was complete, the location and intensity of the diffracted beam was plotted and contoured using multiples of a random distribution (MRD), which is analogous to % per 1% area (Wenk, 1985). The degree of perfection of the fabric (or, the fabric intensity) corresponds to the maximum MRD value, thereby providing a measure of the strength of the fabric. Using a March-type analysis procedure as described by Wood et al. (1976) and Wenk (1985) an ellipsoid can be calculated from each of the stereographic pole figures, which allows for direct comparison of AMS and XTG data. Count times of 4 s per position were used on several samples and the difference between the maximum fabric intensity on 2s and 4s pole figures was <0.2 MRD. A total of one hundred forty-four pole figures were collected from 62 analyses on 33 XTG samples cut from 7 hand specimens.

2.4. X-ray diffraction

Trimmings from samples for AMS and XTG analysis were used for XRD measurements. They were placed in beakers and allowed to soak in distilled water, after which samples were rinsed multiple times to remove salts. Small amounts of powdered sodium carbonate were

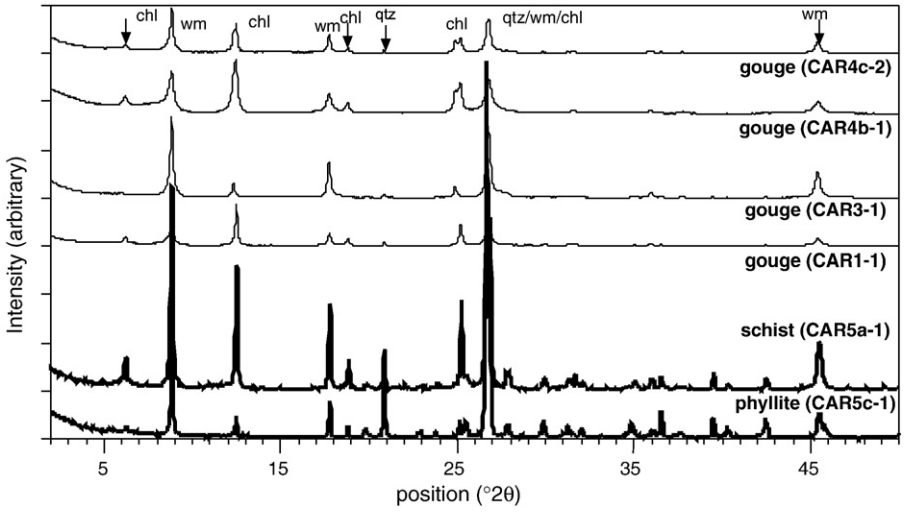

Fig. 2. Representative X-ray powder diffraction patterns of gouge and protolith samples. The gouge samples are dominated by white mica (illite) and chlorite with minor quartz. The mica schist and phyllite contain white mica (muscovite), chlorite and quartz. The labeled peaks are chlorite (chl), white mica (wm), and quartz (qtz). Peaks with multiple labels are peaks shared by multiple phases. The peak widths at half maximum are greater in the gouge than in the protolith, indicating that the grain size in gouge is smaller.

added to promote defloculation (see Moore and Reynolds, 1997). In order to remove coarse non-clay grains gravity settling was used to remove particles greater than 5 μm from suspension, and the <5 μm fraction was decanted. This slurry was then slowly dried under a heat lamp.

XRD samples were prepared such that a preferred orientation of clay grains was created by dumping a clay/water slurry on a glass slide, thereby causing the clay grains to become aligned parallel to the slide (Moore and Reynolds, 1997). This enhances the intensity of the (00l) peaks, aiding in the identification of clay phases. Samples were analyzed on a Scintag X-1 θ–θ powder diffractometer with an accelerating voltage of 35 kV and a filament current of 20 mA from 2 to 50 °2θ at a scan rate of 0.25 °/min. Seven samples (five of gouge, one of mica schist, and one of phyllite) were studied in this fashion.

3. Results

3.1. X-ray diffraction

The gouge samples are composed of chlorite and white mica (mostly illite, although the exact proportions of illite and muscovite were not quantified), and quartz; the phyllite and mica schist are composed of muscovite (visible in hand sample) with lesser amounts of chlorite and quartz (Fig. 2). The peak full width at half maximum (FWHM) values, a function of grain size and number of smectite interlayers (see Merriman and Peacor, 1999), for the 001 illite/muscovite peak (~10 Å/1 nm) are 0.18° in the schist and 0.12° in the phyllite and have values of 0.16–0.3° (average of 0.21°) in gouge indicating the size of the scattering domains is smallest in the gouge, and supporting the idea that fault-related changes in mineralogy have occurred. Very little to no swelling clays (i.e., mixed-layer illite–smectite) were detected, supporting the observations of Faulkner and Rutter (2001).

3.2. Magnetic susceptibility

3.2.1. Temperature dependant susceptibility

Most gouge samples exhibit an increase in bulk susceptibility (~60–15 SI) with decreasing temperature, with an average ratio of K_{293}/K_{77} of ~4.25 (Fig. 3). This temperature/susceptibility relationship indicates that the gouge is dominated by paramagnetic phases, such as chlorite and illite (Richter and van derPluijm, 1994). The paramagnetic dominance indicates, therefore, that AMS provides direct information about clay fabrics, as discussed below. The susceptibility of three samples decreases by only an average ratio of ~3.35, and exhibited atypical fluctuations in susceptibility at low temperature (gray curves on Fig. 3), which may reflect the presence of magnetite. These samples were therefore excluded, as it is not possible to account for the influence of non-paramagnetic phases on the AMS ellipsoid. The samples of phyllite and mica schist contain less paramagnetic material (clays) than gouge samples (with the exception of one gouge sample), indicated by susceptibility of these samples that approaches the K_0 value more quickly than in gouge. The sudden increase in K_0/K at near-room temperature (Fig. 3) is likely due to the melting of ice, resulting in a change in sample volume, and therefore in susceptibility. Data from this range of temperatures were therefore discarded.

3.2.2. Anisotropy of magnetic susceptibility

The AMS ellipsoid is defined by the orientation and magnitude of the maximum (K_1), intermediate (K_2) and minimum (K_3) susceptibilities. AMS ellipsoids for gouge samples are oblate with values of $T = 0$–1 and $P' = 1.05$–1.0 (Fig. 4A), using the parameters of Jelinek (1976). The minimum susceptibility axis parallels the pole to the fault surface, and the maximum axis is parallel to fault strike. The AMS ellipsoid in the phyllite is generally oblate with $T = -0.01$–0.4 and $P' =$ 1.3–1.4; the minimum axis parallels the pole to the foliation and the maximum axis parallels the dip (Fig. 5). In the mica schist the minimum AMS axis is approximately parallel to the dip of the foliation, while to the pole to the foliation approximately bisects the maximum and intermediate axes. In addition 3 of 6 samples are prolate ($T = -0.082$ to -0.021). This indicates that AMS data do not always reflect a single

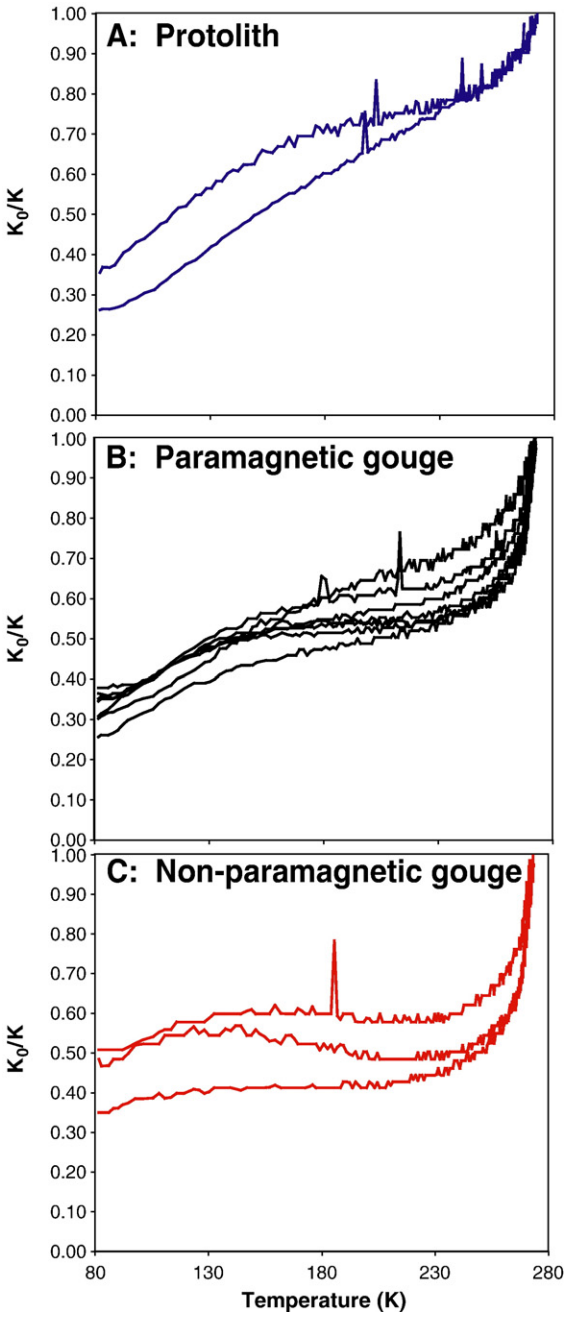

Fig. 3. Temperature dependent susceptibility of gouge and protolith samples. A is protolith, B is paramagnetic gouge, C is non-paramagnetic gouge. K_0/K is the ratio of the susceptibility at a given temperature to the susceptibility at room temperature (293 K). K_0/K for paramagnetic samples increases linearly with temperature, while K_0/K for ferrimagnetic samples does not. The gouge samples are grouped into those dominated by paramagnetic phases (samples for which K_0/K generally increases with temperature) and non-paramagnetic phases (samples for which K_0/K generally remains constant or decreases with temperature). AMS fabrics for the paramagnetic group reflect clay fabrics, while AMS fabrics for the non-paramagnetic group reflect some combination of clay and non-clay phases. The analyses from the non-paramagnetic samples were not used for fabric characterization as it is not possible to remove the non-clay contribution to the anisotropy. The protolith is dominated by paramagnetic behavior, and so it is appropriate to use AMS ellipsoids to characterize clay fabrics in those samples.

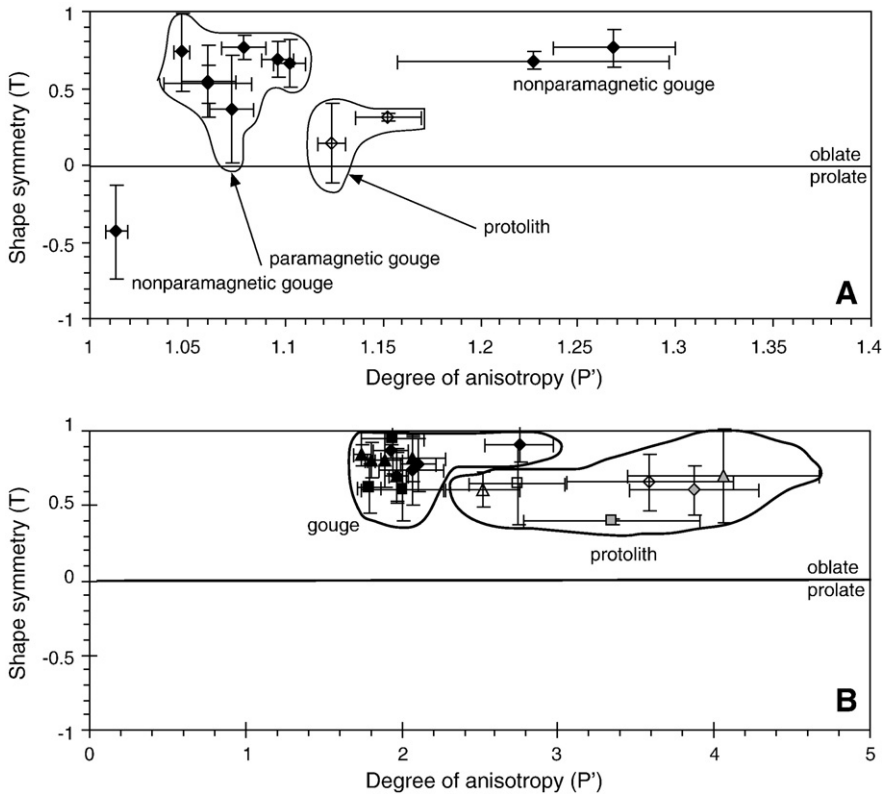

Fig. 4. Fabric shape and intensity plots of Carboneras Fault AMS (A) and XTG (B) measurements. Paramagnetic gouge and protolith fabrics are oblate, and the degree of anisotropy is always greater in phyllite and mica schist protolith than in fault gouge. Samples labeled "non-paramagnetic gouge" in (A) exhibit atypical temperature vs. susceptibility behavior (see Fig. 3). XTG fabrics (open symbols are white mica, gray symbols are chlorite) are markedly more intense than AMS fabrics, and are slightly more oblate. This suggests that fabrics at the mm scale of the XTG measurements are more developed than at the cm scale of the AMS measurements. Error bars represent the range of values for each sample.

clay fabric, but can be controlled by the intersection of two fabrics, as has been shown earlier (e.g., Housen et al., 1993).The schist has average values of T~0.3 and P' = 1.14–1.17 (Fig. 4A). The degree of anisotropy is less in gouge than in protolith, indicating that fabrics in the gouge are less well-developed than in either the phyllite or the schist host rocks.

Sample from gouge with a non-paramagnetic component also exhibit non-typical AMS ellipsoids (P' = 1.013 to 1.268) (T = −0.44 to 0.76). The clay fabrics in these samples are not further characterized since the paramagnetic and non-paramagnetic contributions to the fabric cannot be adequately separated.

3.3. X-ray texture goniometry

Similar to XTG studies of clay fabrics in other fault zones (e.g., Yan et al., 2001; Solum et al., 2003, 2005) the fabric intensity in the Carboneras Fault is low, but occasionally as high as ~7 m.r.d. (ranging 2–7 m.r.d.), whereas the fabric intensity in the mica schist and phyllite protolith is systematically greater (4–13 m.r.d). Illite and chlorite fabric intensities in gouge samples are similar. XTG ellipsoids in gouge are oblate with a shape factor T = 0.4–1 and a degree of anisotropy factor P' ~1.7–2.2 (Fig. 4). Similar to the AMS results, the minimum axis of the XTG ellipsoid is the pole to the fault plane/foliation, while the maximum is subparallel to strike (Fig. 6). This relationship is less pronounced than in AMS analysis, due to the smaller analysis size of XTG, so is more sensitive to small perturbations in the fabric that may occur, for example, by the presence of clasts.

Fabrics of the mica schist and phyllite protolith are oblate with average values of T = 0.4–0.7 and P' = 2.5–4.1 (Fig. 4B), with the minimum susceptibility axis parallel to the pole to foliation, and the maximum is parallel to dip. The pole figures from the mica schist are difficult to interpret due to the large grain size of micas, which are often visible to the naked eye. This effect is shown by the occurrence of multiple discrete peaks on pole figures, each of which has a large intensity (~10 m.r.d.). Analogous to AMS results, the degree of anisotropy is greater in the protolith than in the gouge; however, within protolith the mica fabric intensity (7–13 m.r.d.) is greater than that of chlorite (~4–6 m.r.d.).

4. Discussion

The change in mineral assemblages from protolith, containing chlorite, biotite and muscovite, to illite and chlorite-bearing gouge indicates that fault-related neomineralization has occurred along the Carboneras Fault. Another indication of authigenesis is given by the differences in susceptibility between gouge and protolith that indicate that the gouge contains more of a paramagnetic component (clays) than the protolith. Similar to other clay gouges, samples from the Carboneras Fault are foliated, with many of the foliations defined by polished slip surfaces. The difference between gouge and protolith fabrics, as recorded by both AMS and XTG, indicates that associated fault-related fabric development (related to authigenesis and mechanical processes) has occurred. Since the gouge along this section of the Carboneras Fault is composed (largely) of fault-related clays with fault-related clay fabrics, quantification of the fabrics provides understanding of the ways in which clays can influence fault properties and behavior. XTG fabrics in the gouge are more intense than AMS fabrics (P' = 1.06–1.09 for AMS vs. 1.80–2.75 for XTG), and slightly more oblate (T = 0.36–0.7 for AMS vs. 0.61–0.95 for XTG), indicating that the clay fabrics at the scale of the XTG measurements (~1–2 mm^3) are more intense than at the scale of the AMS measurements (~1000 mm^3). The scatter in the fabric orientations is greater at the smaller XTG scale than at the larger AMS scale. Coupled with the observation that clay fabrics in fault rocks measured using XTG are quite weak compared to most fabrics measured in shales and slates (Solum et al., 2005), this is an indication that preferred orientation of

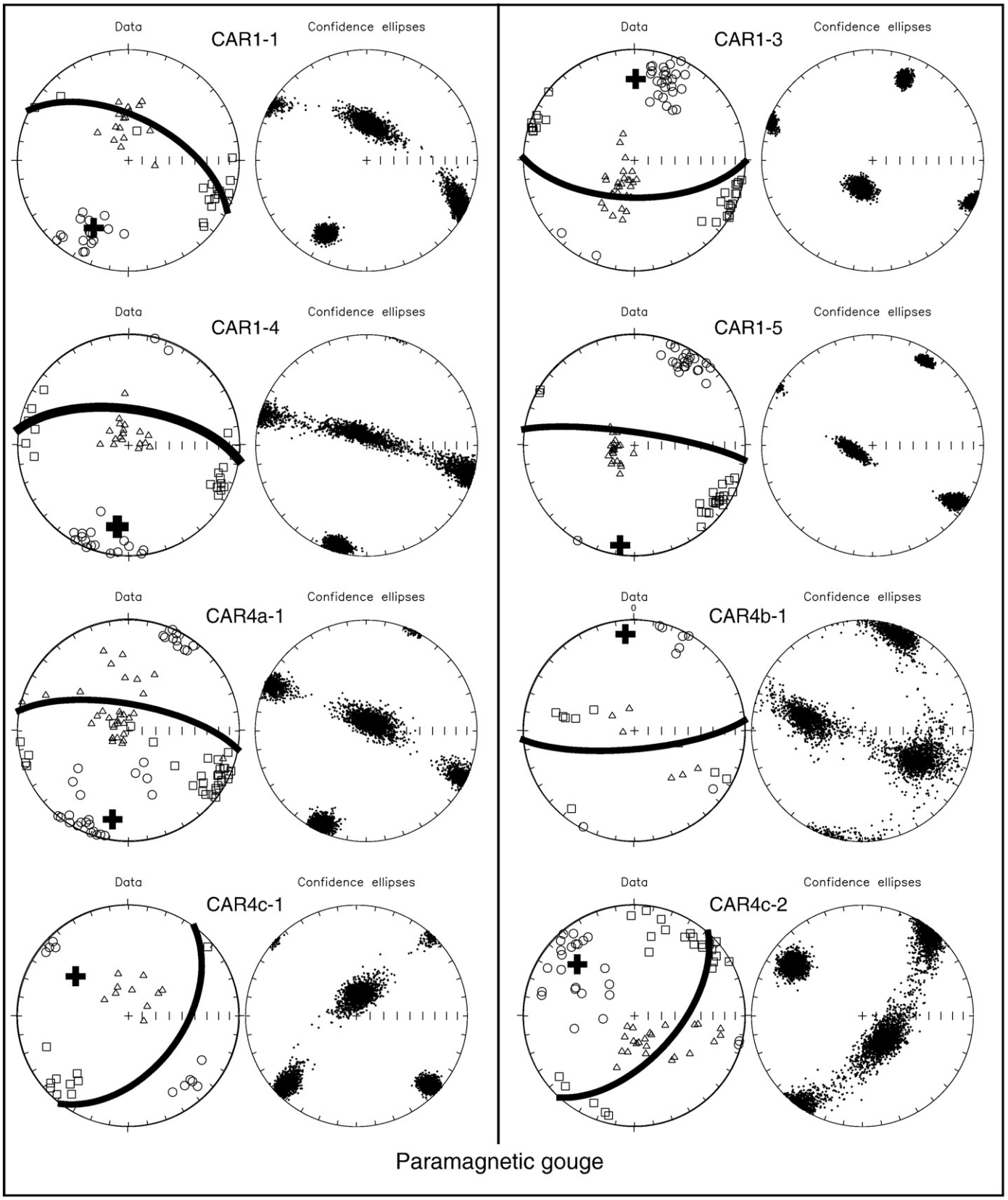

Fig. 5. AMS lower hemisphere, equal area stereographic projections for paramagnetic gouge, paramagnetic + ferromagnetic gouge, and protolith. Each sample is represented by two stereoplots. The left plot shows individual data while the right shows confidence ellipses. The hand sample foliation, plotted as both a pole (heavy cross) and a great circle (heavy line), is generally subparallel to the fault foliation except in two non-paramagnetic gouge samples and in the schist. Squares are the maximum, triangles the intermediate, and circles the minimum susceptibility axes.

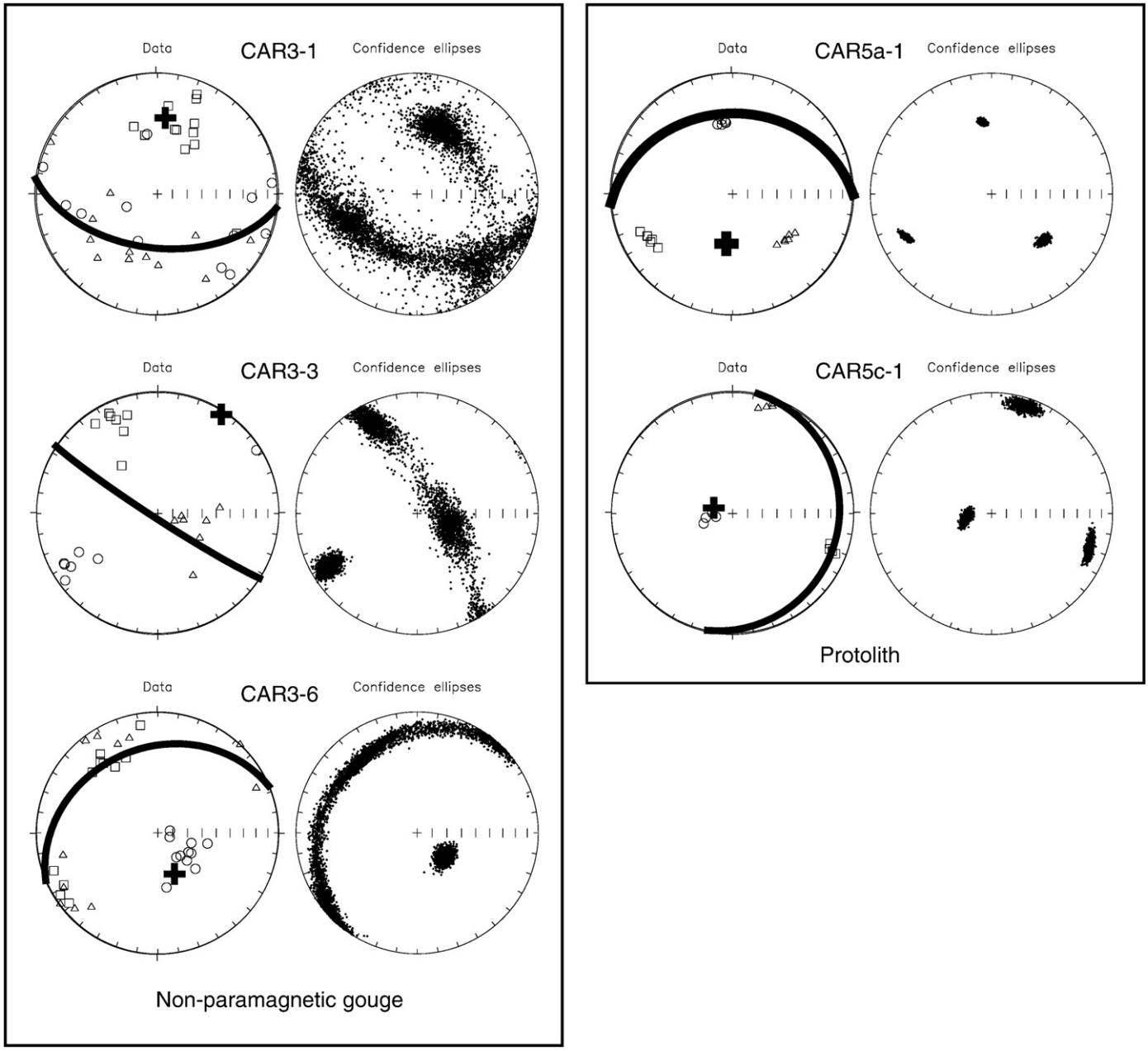

Fig. 5 (*continued*).

clays and intense fabrics in fault rocks are localized phenomena (existing at or below the millimeter scale), visual observations of scaly fabrics or foliations in clay gouge notwithstanding.

The permeability structure of the Carboneras Fault at the location of this study has been characterized in detail by other workers. Faulkner and Rutter (2001) found that the maximum permeability of ~10^{-18} m^2 occurred in the fault plane in a vertical direction (i.e., subparallel to dip), while the minimum permeability of ~10^{-21} m^2 was perpendicular to the fault (i.e., the pole to the fault plane). The orientation of this permeability anisotropy contrasts with both the AMS and XTG fabrics reported here, in which the maximum susceptibility axis is subparallel to strike, indicating that the permeability structure of this very clay-rich fault is not controlled purely by preferentially oriented clays (Faulkner and Rutter (2001) propose that maximum permeability is controlled by elongate fault-parallel quartz stringers that are surrounded by gouge, limiting lateral fluid loss). Two dominant fault-weakening mechanisms are elevated pore fluid pressured and a reduced coefficient of friction. Clays contribute to both. The overall low degree of preferred orientation is compatible with recent observations of active and abandoned members of the San Andreas Fault System at the location of the San Andreas Fault Observatory at Depth (SAFOD) where thin coatings of clays (Solum and van der Pluijm, 2004; Schleicher et al., 2006; Solum et al., 2006) significantly reduce the frictional properties of that system (Tembe et al., 2006; Morrow et al., 2007). The mechanisms controlling the formation of these fine features are not yet constrained, and is part of continued study.

Comparing clay fabrics of the Carboneras Fault to other faults shows that fault rocks from the Punchbowl Fault (Solum et al., 2003), from the Lewis Thrust (Yan et al., 2001) and the Moab Fault (Solum et al., 2005) show poor fabric development relative to their host rocks, with fabric intensities similar to those measured in the Carboneras Fault. Gouge samples from these fault systems contain mixtures of illite, chlorite, with some kaolinite, montmorillonite and mixed-layer illite/montmorillonite in varying proportions, which is mineralogically similar to

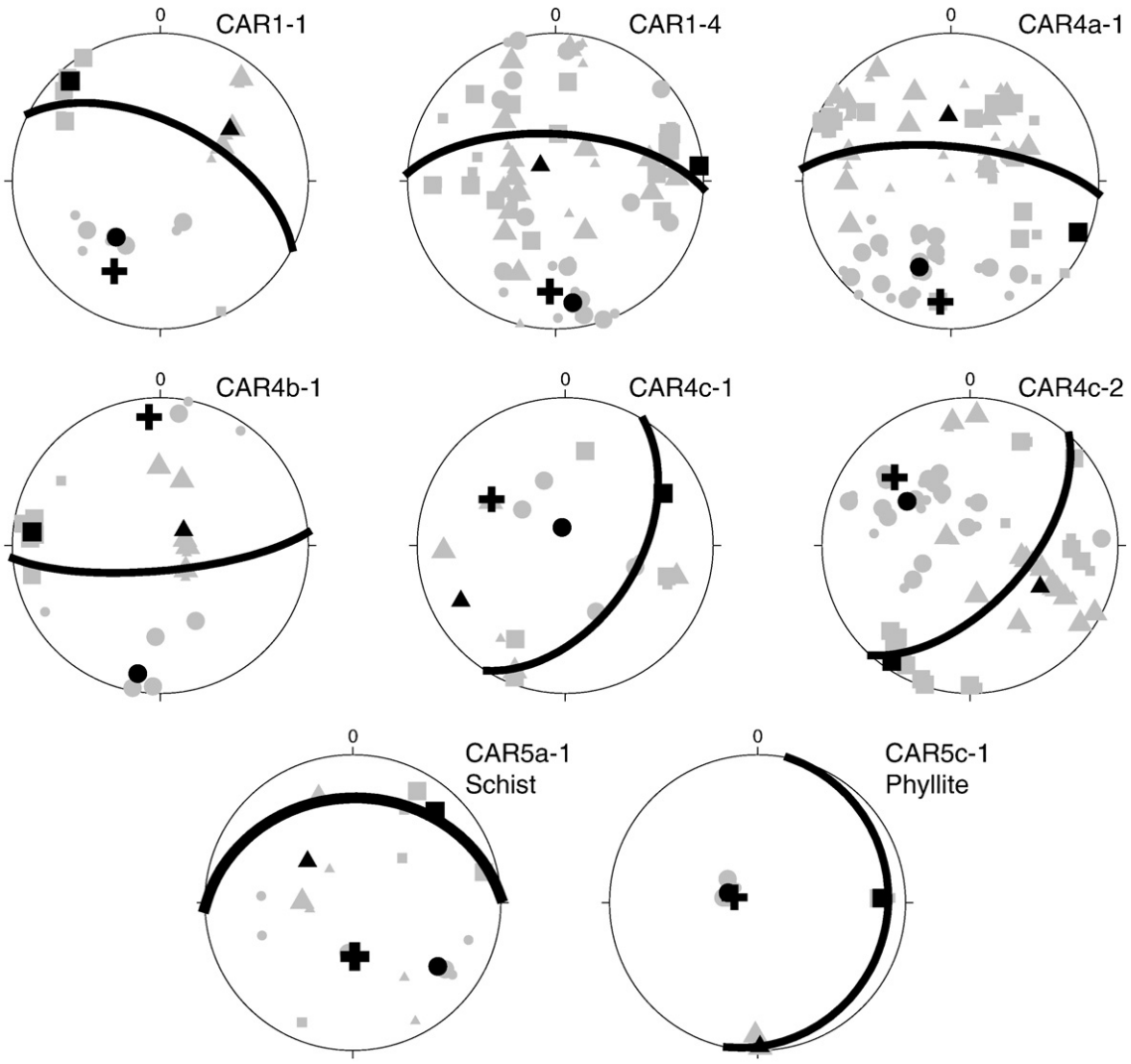

Fig. 6. XTG lower hemisphere, equal area stereographic projections. The measured hand sample foliation is plotted as a great circle (heavy line) and a pole (heavy cross). Phyllite and mica schist are plotted at the bottom of the figure. Black symbols are average values. Large gray symbols represent illite and small gray represent chlorite. As with AMS, the minimum axis (circle) in gouge is approximately parallel to the pole to foliation while the maximum axis (square) is subhorizontal subparallel to strike. The schist shows considerable scatter due to the large size of the mica grains. Given the ~1 mm beam diameter for XTG analysis, coarse-grained samples cannot be reliably quantified.

the Carboneras Fault. While the Carboneras Fault may be broadly similar to other fault zones, the unusually thick clay gouge along that fault represents a very striking difference from other faults. Gouge zones along the Carboneras Fault are atypically wide, being comprised of multiple bands up to ~100 m thick (Faulkner et al., 2003), in contrast to other gouge zones that are usually less than several meters wide (e.g., Chester and Logan, 1986; Evans and Chester, 1995; Chester and Chester, 1998; Foxford et al., 1998; Wilson et al., 2003; Solum et al., 2005, 2006). This difference affects permeability structure as wider gouge zones limit lateral fluid loss out of fault zones (Faulkner and Rutter, 2001). Assuming that similar mineral assemblages and clay fabrics translate to similar permeability anisotropies (i.e., ~3 order of magnitude) this suggests that while the clay mineral assemblages and clay fabrics of the Carboneras Fault are similar to other clay-rich fault zones, the thickness of its gouge zone is not. For elevated fluid pressure to significantly weaken faults containing clay gouge, that gouge must be tens of meters thick, which is much thicker than normally observed. This would suggest that elevated fluid pressure may not be responsible for the weakness of large faults, or at least is not a primary fault-weakening mechanism of crustal-scale faults. This observation is compatible with recent observations from SAFOD, which found no indication of elevated fluid pressure in the fault zone at depth (Hickman et al., 2005).

5. Conclusions

Two dominant fault-weakening mechanisms are elevated pore fluid pressure and a reduced coefficient of friction, and clays contribute to both. The results from this study show that clay authigenesis, and the fabrics of thin coatings of neoformed, frictionally-weak fault-related clays, likely play an important role in controlling the mechanical behavior of (many?) faults. Clay fabrics impart anisotropy of permeability to the permeability structure of fault zones, aiding the maintenance of elevated pore fluid pressure but this appears to be important only when clay gouge zones are unusually (tens of meters) thick. This suggests that weak faults may be due more to the formation of frictionally-weak phases than elevated fluid pressure.

Acknowledgements

Dan Faulkner and Ernest Rutter are thanked for invaluable assistance in selecting sampling locations along the Carboneras Fault and sharing their insights. Josep Pares guided AMS laboratory analysis and provided generous advice and discussion. Funding was provided by NSF grants EAR 9614407 and 0230055 (BvdP), and the Scott M.

Turner Fund at the University of Michigan and a student grant from the American Association of Petroleum Geologists (JGS).

References

Blanpied, M.L., Lockner, D.L., Byerlee, J.D., 1992. An earthquake mechanism based on rapid sealing of faults. Nature 358, 574–576.

Byerlee, J.D., 1993. Model for episodic flow of high-pressure water in fault zones before earthquakes. Geology 21, 303–306.

Chester, F.M., Chester, J.S., 1998. Ultracataclasite structure and friction processes of the Punchbowl fault, San Andreas system, California. Tectonophysics 295, 199–221.

Chester, F.M., Logan, J.M., 1986. Implications for mechanical properties of brittle faults from observations of the Punchbowl Fault Zone, California. Pure Appl. Geophys. 124, 79–106.

Evans, J.P., Chester, F.M., 1995. Fluid-rock interaction in faults of the San Andreas system; inferences from San Gabriel Fault rock geochemistry and microstructures. J. Geophys. Res. 100, 13,007–13,020.

Faulkner, D.R., Rutter, E.H., 1998. The gas permeability of clay-bearing fault gouge at 20 °C. In: Jones, G., Fisher, Q.J., Knipe, R.J. (Eds.), Faulting, Fault Sealing and Fluid Flow in Hydrocarbon Reservoirs. Geological Society Special Publications, London, pp. 147–156.

Faulkner, D.R., Rutter, E.H., 2001. Can the maintenance of overpressured fluids in large strike-slip fault zones explain their apparent weakness? Geology 29, 503–506.

Faulkner, D.R., Lewis, A.C., Rutter, E.R., 2003. On the internal structure and mechanics of large strike-slip fault zones: field observations of the Carboneras Fault in southeastern Spain. Tectonophysics 367, 235–251.

Foxford, K.A., Walsh, J.J., Watterson, J., Garden, I.R., Guscott, S.C., Burley, S.D., 1998. Structure and content of the Moab fault zone, Utah, USA, and its implications for fault seal prediction. In: Jones, G., Fisher, Q.J., Knipe, R.J. (Eds.), Faulting, Fault Sealing and Fluid Flow in Hydrocarbon Reservoirs. Geological Society of London, London, pp. 87–103.

Hayman, N.W., Knott, J., Cowan, D.S., Nesmer, E., Sarna-Wojcicki, A.M., 2003. Quaternary low-angle slip on detachment faults in Death Valley, California. Geology 31, 343–346.

Hickman, S.H., Zoback, M.D., Ellsworth, W.L., 2005. Structure and composition of the San Andreas Fault Zone at Parkfield: initial results from SAFOD Phases 1 and 2. Eos Trans. AGU 86 (52) Fall Meet. Suppl., Abstract T23E-05.

Housen, B.A., Richter, C., van der Pluijm, B.A., 1993. Composite magnetic anisotropy fabrics: experiments, numerical models and implications for the quantification of rock fabrics. Tectonophysics, 220, 1–12.

Hubbert, M.K., Rubey, W.W., 1959. Role of fluid pressure in mechanics of overthrust faulting. Geological Society of America Bulletin 70, 115–166.

Jelinek, V., 1976. The statistical theory of measuring anisotropy of magnetic susceptibility of rocks and its Application. Brno. Geophysika 1–88.

Jelinek, V., 1981. Characterization of the magnetic fabric of rocks. Tectonophysics 79, T63–T67.

Lachenbruch, A.H., Sass, J.H., 1980. Heat flow and energetics of the San Andreas fault zone. J. Geophys. Res. 85, 6185–6222.

Lockner, D., Solum, J.G., Davatzes, N., 2006. The effect of brine composition and concentration on strength of expandable clays. Eos Trans. AGU 87 (52) Fall Meet. Suppl., Abstract T31F-03.

Merriman, R.J., Peacor, D.R., 1999. Very low-grade metapelites: mineralogy, microfabrics and measuring reaction progress. In: Frey, M., Robinson, D. (Eds.), Low-grade metamorphism. Blackwell Science. 313 p.

Moore, D.M., Reynolds Jr., R.C., 1997. X-ray Diffraction and the Identification and Analysis of Clay Minerals. Oxford University Press, New York. 378 pp.

Morrow, C.A., Shi, L.Q., Byerlee, J.D., 1984. Permeability of fault gouge under confining pressure and shear stress. J. Geophys. Res. 89, 3193–3200.

Morrow, C., Solum, J., Tembe, S., Lockner, D., Wong, T.F., 2007. Using drill cutting separates to estimate the strength of narrow shear zones at SAFOD. Geophys. Res. Lett. 34, L11301. doi:10.1029/2007GL029665.

Mount, V., Suppe, J., 1987. State of stress near the San Andreas fault: implications for wrench tectonics. Geology 15, 1143–1146.

Pares, J.M., van der Pluijm, B.A., 2002. Phyllosilicate fabric characterization by low-temperature anisotropy of magnetic susceptibility (LT-AMS). Geophys. Res. Lett. 29, 2215. doi:10.1029/2002GL015459.

Rice, J.R., 1992. Fault stress states, pore pressure distributions, and the weakness of the San Andreas Fault. In: Evans, B., Wong, T.-f. (Eds.), Fault Mechanics and Transport Properties of Rocks; A Festschrift in Honor of W. F. Brace. Academic Press, San Diego, CA, pp. 475–503.

Richter, C., van derPluijm, Ben A., 1994. Separation of paramagnetic and ferrimagnetic susceptibilities using low temperature magnetic susceptibilities and comparison with high field methods. Phys. Earth Planet. Inter. 82, 113–123.

Saffer, D.M., Marone, C., 2003. Comparison of smectite and illite frictional properties: application to the updip limit of the seismogenic zone along subduction megathrusts. Earth Planet. Sci. Lett. 215, 219–235.

Sibson, R.H., 1990. Conditions for fault-valve behaviour. In: Knipe, R.J., Rutter, E.H. (Eds.), Deformation Mechanisms, Rheology and Tectonics, pp. 15–28.

Solum, J.G., van der Pluijm, B.A., 2004. Phyllosilicate mineral assemblages of the SAFOD pilot hole and comparison with an exhumed segment of the San Andreas Fault System. Geophys. Res. Lett. 31, L15S19. doi:10.1029/2004GL01990.

Solum, J.G., van der Pluijm, B.A., Peacor, D.R., Warr, L.N., 2003. The influence of phyllosilicate mineral assemblages, fabrics, and fluids on the behavior of the Punchbowl Fault, southern California. J. Geophys. Res. 108, 2233. doi:10.1029/2002JB001858.

Solum, J.G., van der Pluijm, B.A., Peacor, D.R., 2005. Neocrystallization, fabrics and age of an exposure the Moab fault, Utah. J. Struct. Geol. 27, 1563–1576.

Solum, J.G., Hickman, S.H., Lockner, D.A., Moore, D.E., van der Pluijm, B.A., Schleicher, A., Evans, J.P., 2006. Mineralogical characterization of protolith and fault rocks from the SAFOD main hole. Geophys. Res. Lett. 33, L21314. doi:10.1029/2006GL027285.

Schleicher, A.M., van der Pluijm, B.A., Solum, J.G., Warr, L.N., 2006. Origin and significance of clay-coated fractures in mudrock fragments of the SAFOD borehole. Geophys. Res. Lett. 33, L16313. doi:10.1029/2006GL026505.

Tauxe, L., 1998. Paleomagnetic Principles and Practice. Kluwer Academic Publishers. 299 p.

Tembe, S., Lockner, D.A., Solum, J.G., Morrow, C., Wong, T.-f., Moore, D.E., 2006. Frictional strength of cuttings and core from SAFOD drillhole phases 1 and 2. Geophys. Res. Lett. 33, L23307. doi:10.1029/2006GL027626.

van der Pluijm, B.A., Ho, N.-C., Peacor, D.R., 1994. High-resolution X-ray texture goniometry. J. Struct. Geol. 16, 1029–1032.

Vrolijk, P., van der Pluijm, B.A., 1999. Clay gouge. J. Struct. Geol. 21, 1039–1048.

Wenk, H.-R., 1985. Preferred Orientation in Deformed Metals and Rocks: An Introduction to Modern Texture Analysis. Academic Press, Inc., Orlando, Florida. 610 pp.

Wilson, J., Chester, J.S., Chester, F.M., 2003. Microfracture analysis of fault growth and wear processes, Punchbowl Fault, San Andreas System, California. J. Struct. Geol. 25, 1855–1873.

Wood, D.S., Oertel, G., Singh, J., Bennett, H.F., 1976. Strain and anisotropy in rocks. Philos. Trans. R. Soc. London, Ser. A 183, 27–42.

Yan, Y., van der Pluijm, B.A., Peacor, D.R., 2001. Deformation microfabrics of clay gouge, Lewis Thrust, Canada: a case for fault weakening from clay transformation. In: Holdsworth, R.E., Strachan, R.A., Magloughlin, J.F., Knipe, R.J. (Eds.), The Nature and Tectonic Significance of Fault Zone Weakening. In: Special Publication 186. Geological Society of London, pp. 103–112.

Zhang, S., Cox, S.F., 2000. Enhancement of fluid permeability during shear deformation of a synthetic mud. J. Struct. Geol. 22, 1385–1393.

Zhang, S., Tullis, T.E., Scruggs, V.J., 1999. Permeability anisotropy and pressure dependency of permeability in experimentally sheared gouge materials. J. Struct. Geol. 21, 795–806.

Zoback, M.D., 2000. Strength of the San Andreas Fault. Nature 405, 31–32.